Microporous bamboo biochar for lithium#sulfur batteries

Author

Gu, Xingxing, Wang, Yazhou, Lai, Chao, Qiu, Jingxia, Li, Sheng, Hou, Yanglong, Martens, Wayde, Mahmood, Nasir, Zhang, Shanqing

Published

2015

Journal Title

Nano Research

Version

Accepted Manuscript (AM)

DOI

https://doi.org/10.1007/s12274-014-0601-1

Template for Preparation of Manuscripts for *Nano Research*

TABLE OF CONTENTS (TOC)

Microporous bamboo biochar for lithium−sulfur battery

Xingxing Gu[1], Yazhou Wang[1], Chao Lai[1], Jingxia Qiu[1], Sheng Li[1], Yanglong Hou[2]*, Wayde Martens[3], Nasir Mahmood[2], and Shanqing Zhang[1]*.

[1] Griffith University, Australia.
[2] Peking University, China.
[3]Queensland University of Technology, Australia.

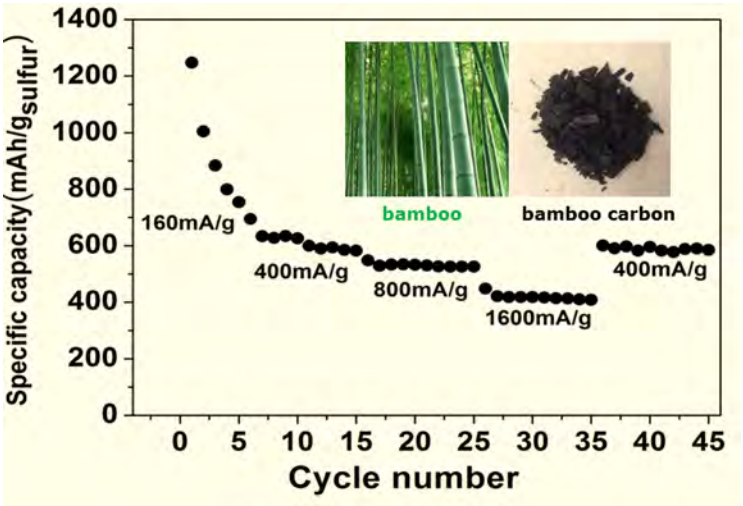

Bamboo biochar has been successfully activated and used to fabricate a porous carbon-sulfur nanocomposite as the cathode material in Li–S batteries. And the bamboo carbon-sulfur nanocomposite cathode illustrates excellent electrochemical performance.

Nano Res
DOI (automatically inserted by the publisher)
Research Article

Microporous bamboo biochar for lithium−sulfur battery

Xingxing Gu[1], Yazhou Wang[1], Chao Lai[1], Jingxia Qiu[1], Sheng Li[1], Yanglong Hou[2](✉), Wayde Martens[3], Nasir Mahmood[2], and Shanqing Zhang[1](✉)

[1] Centre for Clean Environment and Energy, Environmental Futures Research Institute, Griffith School of Environment, Gold Coast Campus, Griffith University, QLD 4222, Australia.
[2] Department of Materials Science and Engineering, College of Engineering, Peking University, Beijing 100871, China
[3] Science and Engineering Faculty, Queensland University of Technology QLD 4001, Australia.

Received: day month year / Revised: day month year / Accepted: day month year

ABSTRACT

Being simple, inexpensive, scalable and environmentally friendly, microporous biomass biochars have been attracting enthusiastic attention for application in lithium-sulfur (Li–S) batteries. Herein, porous bamboo biochar is activated via a KOH/annealing process that creates a microporous structure, boosts surface area and enhances electronic conductivity. The treated sample is used to encapsulate sulfur to prepare microporous bamboo carbon-sulfur (BC-S) nanocomposite as the cathode for Li–S batteries for the first time. The BC-S nanocomposite with 50 wt% sulfur content delivers a high initial capacity of 1295 mAh/g at a low discharge rate of 160 mA/g and high capacity retention of 550 mAh/g after 150 cycles at a high discharge rate of 800 mA/g with excellent coulombic efficiency (≥95%). This suggests that the BC-S nanocomposite could be a promising cathode material for Li–S batteries.

KEYWORDS

biochars, lithium-sulfur batteries, microporous structure, bamboo carbon-sulfur composites

1 Introduction

Nowadays rechargeable lithium batteries (LIBs) have been playing a predominant role in current portable electronics, such as smartphones, laptops, and digital cameras and so on. However, there are still several barriers that need to be overcome to enable their applications in electric vehicles (EVs) and hybrid electric vehicles (HEVs), such as high cost, limited energy capacity and insufficient energy density. Therefore, there are increasing interests in research and development of LIBs to meet the demands of power sources for the EVs and HEVs. In comparison with traditional cathode materials, such as $LiCoO_2$ and $LiMn_2O_4$, sulfur has high theoretical specific capacity of 1675 mAh/g and energy density of 2600 Wh/kg as well as its high abundance, nontoxicity and inexpensiveness make it an attractive alternative[1-3]. Therefore Li–S batteries have attracted enormous attention worldwide for the

Address correspondence to email1: s.zhang@griffith.edu.au; email2: hou@pku.edu.cn

next generation of LIBs

However, it's well recognised that the commercialization of the Li–S batteries is mainly hindered by the low utilization and rapid capacity decay of the pure sulfur due to three factors: 1) the inherently poor electrical conductivity of sulfur (5×10^{-30} S/cm at 25 °C)[4, 5]; 2) significant structure and volumetric changes during the charge/discharge process[6]; 3) polysulphides readily dissolve in the organic electrolyte, shuttle to anode and then react with lithium during the charging process, resulting in deposition of insulating Li_2S_2/Li_2S at the electrode interface and causing the electrical and ionic mass transfer blockage[4, 5]. Therefore, a variety of strategies including electrolyte development[7], anode modifications[8], inserting interlayer[9], and cathode synthesis[10-12] etc., have been intensively investigated in order to address the above issues in the charge/discharge processes. In particular, the sulfur-micro/mesoporous carbon (S–MPC) composites have been regarded as one of the most promising Li–S cathodes[4-6, 10-17]. To date, although significant improvements in terms of rate capability and stability have been achieved, practically the aforementioned restrictions of the Li–S batteries remain unsolved. The synthesis process of porous carbon materials, such as CMK-3[10], is commonly sophisticated and therefore costly, and lacks scalability and consistency. Thus, it is necessary to find highly efficient and low cost porous carbon to build high performance sulfur-based composites.

Porous biochar, derived from the biomass, has drawn increasing attention because they are inexpensive, readily available, environmentally friendly, and sustainable[4, 18]. To date there have been various kinds of porous biochar reported as the sulfur host for Li–S batteries[4, 6, 19-22]. Bamboo as a natural biomass is extensively used in everyday live due to its excellent sustainability i.e., fast growth and short maturity cycle[18]. Most importantly, the bamboo has unique well-connected three-dimensional (3D) microtexture that can be carbonized into a hierarchical porous carbonaceous structure, which possesses large surface area, high conductivity, well-connected and highly ordered structure[18]. Therefore, bamboo biochar is currently available as an odour absorbent and has also been used to fabricate electrodes for supercapacitors and LIBs[18, 23-26].

In this work, a commercially available and low cost bamboo biochar is used as bamboo carbon (BC). The BC sample is treated by a simple KOH/annealing strategy as shown in scheme 1. The treated BC (T_BC) is used to synthesize microporous bamboo carbon-sulfur (T_BC-S) nanocomposites with various sulfur contents. The T_BC-S electrode shows better performance in comparison with a pristine BC-S electrode. The mechanisms responsible for the increased performances are systematically investigated using cyclic voltammetry (CV), galvanostatic charge-discharge, and electrochemical impedance spectra (EIS).

2. Experimental

2.1 Samples preparation

The activation of BC: commercial bamboo carbon is firstly grinded at 500 rpm for 3 hours by planetary ball mill (QM-3SP04, Nanjing Nanda Instrument Plant) and sieved with a 400 mesh sieve and designated ball milled bamboo carbon (B_BC). Secondly, the B_BC is immersed into an 8 M KOH (analytical reagent, Sigma-Aldrich) solution for 16 h. After drying, it is annealed at 700 °C for 2 hours under an Ar atmosphere for activation. The T_BC is collected by centrifugation, and washed with 1M HCl solution and distilled water to remove residual KOH. The washed T_BC is then dried in vacuum oven at 60 °C overnight.

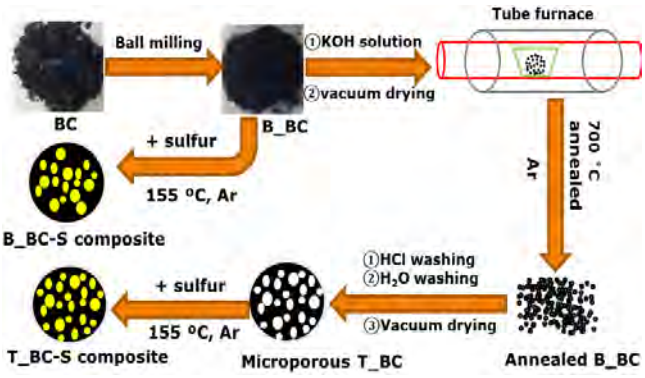

Scheme 1 The preparation process of T_BC-S and B_BC-S composites

The synthesis of B_BC-S and T_BC-S composites: different amounts (i.e., 40%, 50% and 60%) of pure sulfur (analytical reagent, Sigma-Aldrich) are mixed

with the B_BC and T_BC samples, respectively. These mixtures are then sealed into Teflon containers and heated at 155 °C for 12 hours under an Ar atmosphere. After cooling to room temperature, the B_BC-S and T_BC-S composites with different sulfur contents are obtained, namely B_BC-S-50%, T_BC-S-40%, T_BC-S-50%, and T_BC-S-60% samples.

2.2 Samples characterization

The microstructure and morphology of all samples are examined using a JSM-7001F scanning electron microscopy (SEM) (JEOL, Japan) and a Model Tecnai 20 transmission electron microscopy (TEM) (FEI, USA) with an acceleration voltage of 200 kV. Energy dispersive X-ray spectroscopy (EDX) analysis and element mapping are obtained from JSM-6610 (JEOL, Japan). XRD patterns are obtained with an X-ray diffraction (XRD) instrument (Model LabX-6000, Shimadzu, Japan) using CuK_α radiation (λ=1.54Å) at 40 kV and 40 mA over the 2θ range of 10−80°. The specific surface areas and pore volumes of B_BC, T_BC and T_BC-S composites were measured by the Brunauer−Emmett−Teller (BET) method using nitrogen adsorption and desorption isotherms on a Tristar3000 system (Micromeritics, USA). Pore size distribution plot is obtained by Horvath-Kawazoe method from the adsorption branch of the N_2 adsorption/desorption isotherms. Thermogravimetric analyses (TGA) are carried out under an N_2 atmosphere from room temperature to 600 °C on a Series Q500 instrument (TA Instruments, USA) to determine the sulfur loadings in the B_BC-S and T_BC-S composites. Heating rates of 10 °C min^{-1} were used in these TGA experiments.

2.3 Electrochemical measurements

All B_BC-S and T_BC-S samples were mixed with carbon black and polytetrafluoroethylene (PTFE, analytical reagent, Sigma-Aldrich) in a weight ratio of 70: 20: 10, with ethanol (analytical reagent, Sigma-Aldrich) as a dispersant. The pastes are rolled into a film with a rolling pin, and then cut into many pieces of wafers by mould. The wafer is approximately 0.5 cm^2 in area and has an average weight of 2 mg after dried at 60 °C in vacuum oven for 12 hours. The half-cells are assembled with home-made module in a glove box (M-Braun, USA) with high pure argon. This configuration consists of the lithium metal as the counter electrode, polypropylene (Celgard 2300) as the separator, and 1 M LiTFSI in DOL/DME (1:1, v/v) containing 0.1 M $LiNO_3$ as the electrolyte. The calculation of the specific capacity is based on the mass of the sulfur active material. The charge and discharge performances of the half-cells are tested with LAND CT-2001A instrument (Wuhan, China), and the potential range is controlled between 1.5 and 3.0 V at room temperature. CHI 660D electrochemical workstation (CHI Instrument, Shanghai, China) is used to perform the CV with a scan rate of 0.1 mV/s and a potential from 1.5 V to 3 V. The EIS is also recorded using the same instrument over frequency range from 100 kHz to 10 mHz

3. Results and Discussion

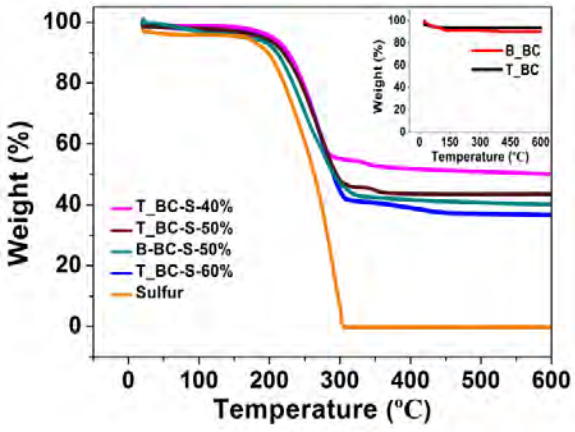

Fig. 1 The TGA thermograms of sulfur, B_BC, T_BC, B_BC-S and T_BC-S composites.

The thermostability of the samples is evaluated by TGA as presented in Fig. 1. It is obvious that no significant weight losses is observed for the B_BC and T_BC (inset of Fig. 1) samples between 200 °C and 600 °C, which suggests that the BC samples are thermally stable in this temperature range. The element sulfur presents typical thermal characteristics, i.e., it starts to vaporize at ca. 200 °C and completes at 300 °C. Therefore, the significant weight losses of the B_BC-S and T_BC-S composites that is observed between 200 °C and 300 °C can be attributed to the evaporation of the absorbed sulfur. Accordingly, the sulfur content in the composites are determined to be 39.5 wt%, 50.1 wt%, 59.7 wt%, and

49.3 wt% for the T_BC-S-40%, T_BC-S-50%, T_BC-S-60% and B_BC-S-50%, respectively, which are consistent with the used amounts of sulfur in the preparation process.

As shown in Fig. 2, the T_BC shows a type I isotherm (a Langmuir-type isotherm), which indicates the characteristic microporous structure of the T_BC[27]. It is worth noting that the T_BC has a narrow pore size distribution, mainly in the range of ca. 0.6 and 0.75 nm as shown in the inset of Fig. 2. The values of BET area and pore volume of the B_BC and T_BC samples are displayed in Table 1. Interestingly, Table 1 suggests that the specific surface area of T_BC has been boosted up for 14 times while the pore volume increased to almost 8 times. This is a remarkable improvement which may be attributed to the proposed chemical process as shown in Eqns (1)-(5)[28].

$$6KOH + 2C \rightarrow 2K + 3H_2 + 2K_2CO_3 \quad (1)$$

$$K_2CO_3 \rightarrow K_2O + CO_2 \quad (2)$$

$$CO_2 + C \rightarrow 2CO \quad (3)$$

$$K_2CO_3 + 2C \rightarrow 2K + 3CO \quad (4)$$

$$C + K_2O \rightarrow 2K + CO \quad (5)$$

It is well known that BC commonly consists of amorphous carbon and graphitic carbon[26]. After the BC is soaked into the concentrated KOH solution, KOH penetrates into entire structure of BC, including the graphitic structure as suggested by the XRD spectrum, shown in Fig. 3. Further on, at high temperature (700 ºC), KOH etches the carbon frameworks and graphitic layer structure according to the various chemical reactions listed above. It is these reactions that are responsible for generating the porous network and opening up the layered graphitic structure[28]. This can be evidenced by the fact that the graphitic peak at 2θ degree of 25.3° cannot be observed for the T_BC sample as shown in the Fig. 3. Instead, a new broad peak between 2θ degree of 40° and 50° suggests the major composition of the T_BC sample has changed to amorphous carbon[6, 19, 21].

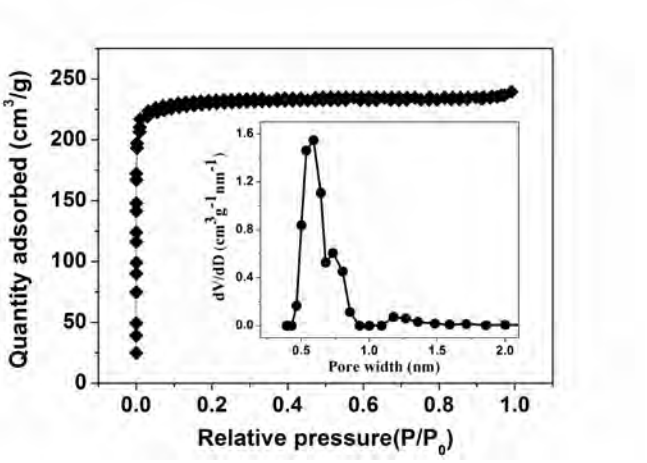

Fig. 2 N_2 adsorption/desorption isotherm with a corresponding pore size distribution of the T_BC

Table 1 Physical characteristic of B_BC and T_BC.

Sample	BET surface area (m^2/g)	Total pore volume (cm^3/g)
B_BC	56.00	0.050
T_BC	791.80	0.380

After sulfur is loaded into the T_BC, the pore volumes and specific surface areas of the T_BC–S composite reduce sharply, i.e. T_BC–S-50%'s specific area and pore volume are only 0.53 m^2/g and 0.003 cm^3/g respectively. This indicates the elemental sulfur is embedded into the micropores of T_BC due to extremely strong physical adsorption[27, 29]. And as shown in the inset of Fig. 3, the lower sulfur loading (i.e., 40 wt%), the weaker characteristic diffraction peaks of the crystalline sulfur can be identified with a low intensity, implying that most of the sulfur diffuse into the pores of the T_BC matrix, and exist in a highly dispersed or amorphous state[30]. In contrast, because the pore volume of B_BC is very small (as shown in Table 1) before the activation process, the sulfur in the B_BC-S-50% composite are mainly distributed on the surface of B_BC when it suffers the heating process, leading to a strong diffraction peaks of the crystalline sulfur.

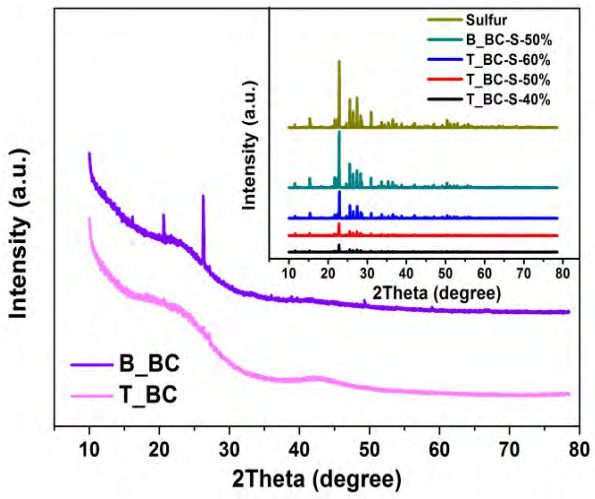

Fig. 3 XRD diffractograms of the sulfur, B_BC, T_BC, B_BC-S and T_BC-S composites.

As shown in Fig. 4a and 4b, the B_BC contains abundant pores range from 0.1μm to 2μm. The pores appear shallow as they are commonly blocked by impurities such as tar[4]. In contrast, after being activated, the pores turn deep in the T_BC because they are unblocked. The surface of T_BC is smoother than that of B_BC, indicating the removal of the impurities. More importantly, these open macropores are in favour of the infiltration of the electrolyte[4]. From Fig. 4d, the T_BC-S-50% has obviously different morphology from those of B_BC and T_BC. After sulfur infiltrating, the abundant pore structures have disappeared, and at the same time, some sulfur particle clusters on the surface of T_BC are observed, indicating that all the pores in the T_BC are saturated with sulfur and the sulfur starts to accumulate at the surface. The observation agrees well with the results of XRD and BET data. The EDX and elemental mapping (Fig. S1) confirm that sulfur particles are distributed homogeneously in the framework of the porous T_BC.

As illustrated in Fig. 4e, the abundant microporous structure with small pore sizes (< 1 nm) of T_BC is observed in the high-resolution TEM image, which is consistent with the N_2 adsorption/desorption results. The developed microporous structure is favourable for both the diffusion of the melted sulfur adsorption during thermal treatment process and the access connection of the electrolyte throughout the porous structure of carbon during cycling. Moreover the micropores in the T_BC act as microporous reactors and restrict the dissolution of lithium polysulfides in organic electrolyte due to the strong physical adsorption[27]. While the high-resolution TEM image of T_BC-S-50% (Fig. 4f) demonstrates the crystal lattice fringes with *d*-spacing of 0.38 nm corresponds to the (222) plane of the element sulfur. Meanwhile it is hardly observed the microporous structure from the Fig. 4f, again suggesting the sulfur has been fully incorporated in the micropores.

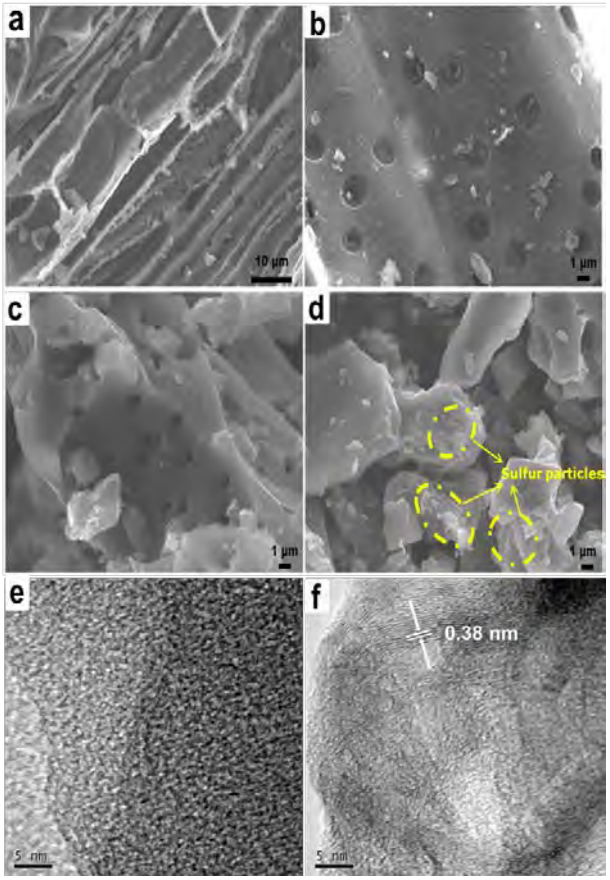

Fig. 4 SEM images of the B_BC (a, b), T_BC (c), T_BC-S-50% (d) and TEM images of the TBC (e), T_BC-S-50% (f).

Cyclic voltammetry experiment is conducted to investigate the electrochemical mechanisms of the as-prepared Li–S batteries. Fig. 5a shows the CV curves of the T_BC-S-50% electrode at a scan rate of 0.1 mV during the first three cycles. In the first cycle of cathode reduction process, three peaks at approximately 2.3 V, 2.1 V, 1.7 V are observed, which correspond to the reduction of elemental sulfur to higher-order polysulphides lithium (Li_2S_x, $4 < x < 8$) and the reduction of higher-order polysulphides

lithium to lower-order polysulphides lithium, even to insoluble Li_2S, respectively[31-33]. In the subsequent anodic scan, one asymmetric oxidation peak (which can be divided into two peaks) is observed at around 2.38 V and attributed to the conversion of lithium sulfides to polysulfides and sulfur[31, 34]. Meanwhile from the second cycle, the position and areas of the CV peaks remain nearly unchanged with cycle number increasing, implying good reaction reversibility and cycling stability of the nanocomposite electrode after the second cycle [31, 34, 35].

Typical voltage capacity profiles of the T_BC-S-50% at various cycles are revealed in Fig. 5b. These discharge curves show two typical plateaus (around 2.3 V and 2.1 V respectively) like all the sulfur-containing electrodes, which could be assigned to a two-step reaction of sulfur with lithium during the discharge process, agreeing well with the results of CV measurements[31, 32, 34]. Commonly, the long sloping plateau below 2.0 V could be observed in the carbonate electrolyte[27, 36]. The long sloping plateau below 2.0 V in Fig. 5b might result from the strong adsorption process of Li_2S_2 on the micropores besides the reduction process (from Li_2S_2 to Li_2S) at around 1.7 V. This observation is similar as other micropours carbon-sulfur composite electrode[33]. Such strong interactions can ensure the stable performance of T_BC-S-50% sample[33]. In addition, as noticed in Fig. 5b, the discharge plateaus are still obvious and stable even after 150 cycles, which also ensures the excellent cyclic performance (550 mAh/g after 150 th) of the nanocomposite cathode.

Fig. 6a and 6b illustrates the cycling performances of B_BC-S and T_BC-S composites at 160 mA/g and 800 mA/g rate, respectively. On the one hand, it demonstrates the cycling performance of T_BC-S-50% electrode is much better than that of B_BC-S-50% when the sulfur loading is literally the same. The mechanism of the strategy can be concluded as follows: 1) the T_BC material has far higher specific area and pore volume of the micropores than the B_BC material, which can provide more active sites and reduce the loss of the active material[6]; 2) the activation process removes the impurities, i.e. tar[4], which are detrimental to the lithium-sulfur cells; 3) the far more micropores of T_BC ensure good electrical contact between sulfur and the conductive carbon framework, further facilitates Li-ions transportation through providing low resistance pathways[18, 22].

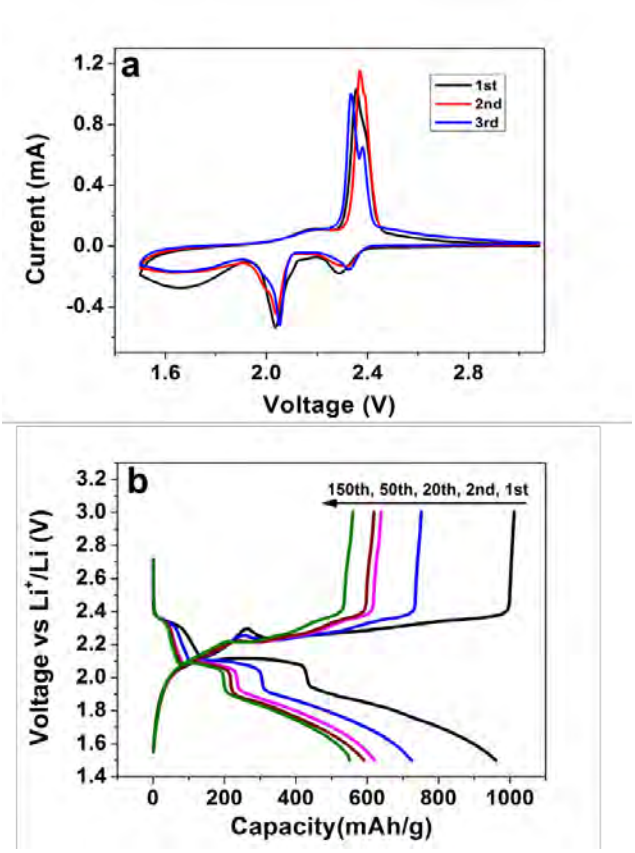

Fig. 5 Cyclic voltammogram of T_BC-S-50% (a) and Galvanostatic charge-discharge curves of the T_BC-S-50% cathode at 800 mA/g (b).

On the other hand, the initial capacity and reversible capacity are first increased and then decreased with the sulfur content increasing while the conductive matrix is fixed as T_BC. For instance, the initial capacity first increases from 856 mAh/g for T_BC-S-40% to 961 mAh/g for T_BC-S-50%, and then dramatically decreases to 618 mAh/g for T_BC-S-60% at 800 mA/g rate. After 150 cycles, the T_BC-S-50% also exhibits the highest reversible capacity with 550 mAh/g, implying the high utilization of the active sulfur in the composite with around 50 wt% sulfur loading[30, 37]. Thus the implication is that the sulfur content embedded into the bamboo carbon can directly impact the overall performance of the nanocomposite. On the one hand, if the sulfur content is too low (e.g, 40% in our case), the intrinsic

polysulphides formed in the charge process can readily dissolve in the organic electrolyte solution, leading to a severe shuttle phenomenon which will cause the lower sulfur utilization [37]. On the other hand, if the sulfur content is too high (e.g, 60% in our case), lower conductivity and insoluble Li_2S_2 or Li_2S can readily be produced during the discharge process, resulting in the lower sulfur utilization percentage and rapid decline of the specific capacity. [37]. Therefore, the sulfur content needs to optimize to address the aforementioned problems. In the case of the T_BC-S-50%, this sample, which contains 50% sulfur content, was found to be the best among all the tested samples.

In fact, the electrochemical performance of T_BC-S-50% is among the best of the Li-S batteries based on other types of biochars as shown in Table 2. In particular, the composite cathode T_BC-S-50% displays the highest initial capacity and the second highest reversible capacity (after 50 cycles) as shown in Table 2. Moreover the sulfur utilization efficiency of our composite cathode is the largest compared to other biochar-sulfur composites cathode.

Furthermore, an excellent rate capability performance is observed in Fig. 6c. After the cell being activated at a 160 mA/g rate for the first 5 cycles, further cycling at 400 mA/g, 800 mA/g, 1600 mA/g rate show reversible capacities of about 600 mAh/g, 540 mAh/g and 410 mAh/g, respectively. When the rate is switched to 400 mA/g again, the electrode resumes the original capacity of approximately 600 mAh/g, indicating the T_BC-S-50% cathode material is highly robust and stable[38].

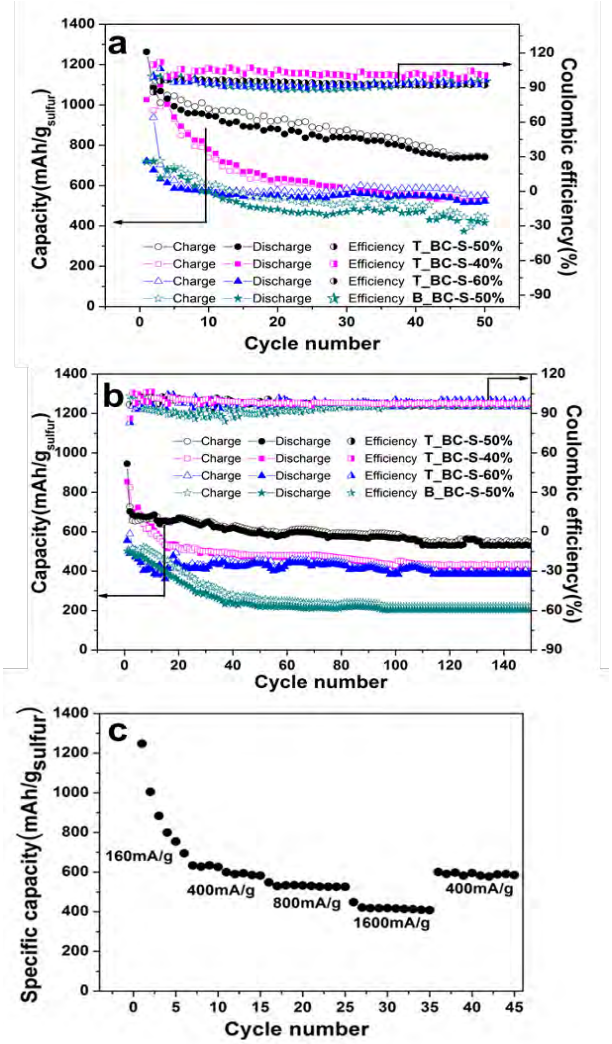

Fig. 6 Cycle life of the B_BC-S and T_BC-S composites at a rate of 160mA/g (a), and 800 mA/g (b), rate capability of T_BC-S-50% electrode (c).

Table 2 Electrochemical performance of Li-S cells basing on different porous biochar carbon

Biochar type	Initial capacity (mAh/g)	50^{th} cycle capacity (mAh/g)	Rate (mA/g)	S (%)	Ref.
Pomelo peels carbon	1280	~880	335	60	4
Pig bone carbon	1265	643	–	–	19
Kapok carbon fibers	549	~524	670	93	21
Olive stone derived carbon	930	670	100	80	22

Bamboo carbon	1295	756	160	50	this work

To better understand the improved electrochemical performances with the use of activated microporous bamboo carbon, the EIS (Fig. 7) of the as-prepared materials before discharge and after 50 cycles are measured. Before discharging, the impedance spectra are composed of a medium-to-high frequency semicircle and a long inclined line (Warburg impedance) in the low frequency region. The semicircle is attributed to the charge-transfer process at the interface between the electrolyte and sulfur electrode. The Warburg impedance is associated with semi-infinite diffusion of soluble lithium polysulfide in the electrolyte[39, 40]. After 50 cycles, the impedance spectra demonstrate two depressed semicircles followed by a short sloping line. The semicircle in the higher frequency region reflect the interfacial charge transfer process, and the semicircle in the medium frequency range is related to the solid-electrolyte-interface (SEI) film which is caused by the formation of Li_2S (or Li_2S_2) on the carbon matrix in the cathode[39, 40]. The equivalent circuit models for analysing impedance spectra are shown in the inset of Fig. 7a and Fig. 7b, respectively. R_e represents the impedance contributed by the resistance of the electrolyte, R_{ct} is the charge transfer resistance at the conductive agent interface, CPE is a constant phase element which is used instead of capacitance and R_s is a deposit diffusion resistance of SEI film. W_c is the Warburg impedance due to the diffusion of the polysulfides within the Cathode[39]. As shown in Fig. 7a and Table 3, the R_{ct} (before discharge) of T_BC-S-50% is much smaller than that of B_BC-S-50%, which could be attributed to the enhanced conductivity of the T_BC-S-50%[6, 21]. And the R_{ct} values increase significantly with increasing the sulfur loading (62.5, 109.3 and 310.0 Ω for the samples with 40 wt%, 50 wt% and 60 wt% S content, respectively), which is mainly due to the fact that the sulfur possesses very high resistance. After 50 cycles, the R_{ct} of all the samples decrease in comparison with that at the beginning, indicating that the irreversible deposition and aggregation of insoluble Li_2S and Li_2S_2 on the surface of the BC-S nanocomposites and transportation of Li-ions becomes much easier as the cycle number increase, which in turn benefits the high rate capability of the cathode during long cycling[35]. After 50 cycles, the R_{ct} of T_BC-S-50% is the smallest, which may be attribute to the highest sulfur utilization and least shuttle phenomenon, which contribute to the T_BC-S-50% nanocomposite cathode demonstrating best performance at long cycle and high charge/discharge rates[41].

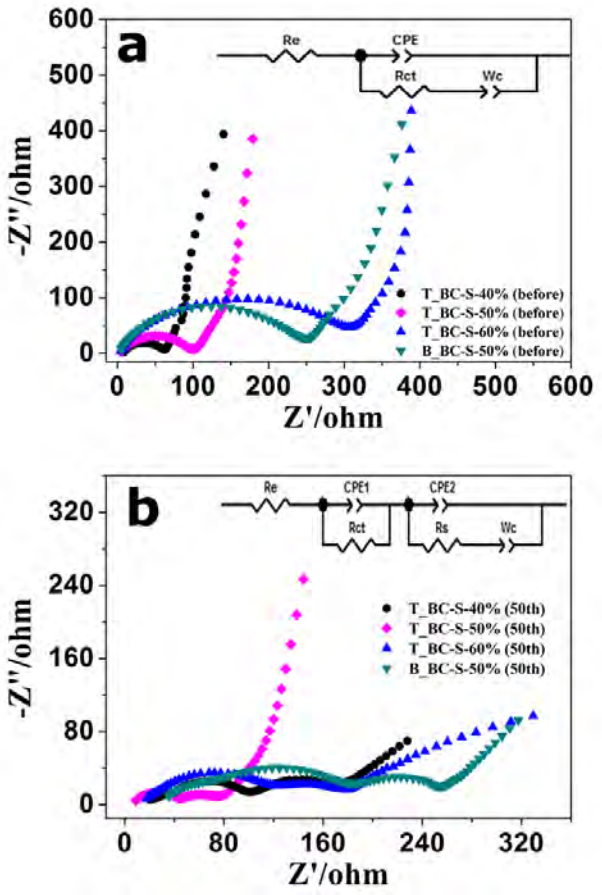

Fig.7 Nyquist plots before discharge (a) and after 50th (b) of B_BC-S and T_BC-S composites

4. Conclusions

Bamboo biochar has been successfully activated and used to fabricate a porous carbon-sulfur nanocomposite as the cathode material in Li–S batteries. This simple and facile activation process

plays a key role in producing the microporous carbon with two functions: It can encapsulate sulfur and polysulphides to reduce the shuttle phenomenon during cycling and at the same time maintain electrical contact between the sulfur and the conductive carbon framework during the charge/discharge process. In addition, after the B_BC being activated, the open macropores and newly added micropores are beneficial to the electrolyte infiltrate into the cathode materials strongly. Therefore, the T_BC-S samples illustrate improved electrochemical performances compared to the B_BC-S sample, among which the T_BC-S-50% sample delivers a high initial capacity of 1262 mAh/g at 160 mA/g and high reversible capacity of 550 mAh/g at as high as 800 mA/g rate with a coulombic efficiency over 95%. Consequently, BC-S composite could be a promising and alternative cathode material for the Li–S batteries.

Table 3 Impedance parameters simulated from the equivalent circuits.

Cycle number	Resistance	T_BC-S-40%	T_BC-S-50 %	T_BC-S-60%	B_BC-S-50%
Before discharge	R_e	4.5	3.6	2.2	2.4
	R_{ct}	62.5	109.3	310.0	239. 4
After 50 cycles	R_e	17.7	6.5	16.4	21.9
	R_{ct}	57.2	35.7	105.5	194.0
	R_s	42.3	39.6	49.9	57.6

Acknowledgements

The authors acknowledge the financial support of the ARC Discovery Grants from the Australian Research Council, the NSFC-RGC Joint Research Scheme (51361165201) and NSFC (51125001, 51172005).

Electronic Supplementary Material: Supplementary material (EDS imaging) is available in the online version of this article at http://dx.doi.org/10.1007/s12274-***-****-*

References

[1] Peramunage, D.; Stuart, L. A solid sulfur cathode for aqueous batteries. *Scinence* **1993,** *261*, 1029–1032.

[2] Bruce, P. G.; Freunberger, S. A.; Hardwick, L. J.; Tarascon, J. M. Li-O_2 and Li-S batteries with high energy storage. *Nature materials* **2012,** *11*, 19–29.

[3] Ji, X.; Nazar, L. F. Advances in Li–S batteries. *Journal of Materials Chemistry* **2010,** *20*, 9821–9826.

[4] Zhang, J.; Xiang, J.; Dong, Z.; Liu, Y.; Wu, Y.; Xu, C.; Du, G. Biomass derived activated carbon with 3d connected architecture for rechargeable lithium−sulfur batteries. *Electrochimica Acta* **2014,** *116*, 146–151.

[5] Jayaprakash, N.; Shen, J.; Moganty, S. S.; Corona, A.; Archer, L. A. Porous hollow carbon@sulfur composites for high-power lithium-sulfur batteries. *Angew Chem Int Ed Engl* **2011,** *50*, 5904–5908.

[6] Zhao, S.; Li, C.; Wang, W.; Zhang, H.; Gao, M.; Xiong, X.; Wang, A.; Yuan, K.; Huang, Y.; Wang, F. A novel porous nanocomposite of sulfur/carbon obtained from fish scales for lithium–sulfur batteries. *Journal of Materials Chemistry A* **2013,** *1*, 3334–3339.

[7] Jeddi, K.; Ghaznavi, M.; Chen, P. A novel polymer electrolyte to improve the cycle life of high performance lithium–sulfur batteries. *Journal of Materials Chemistry A* **2013,** *1*, 2769–2772.

[8] Lee, J. H.; Lee, H. Y.; Oh, S. M.; Lee, S. J.; Lee, K. Y.; Lee, S. M. Effect of carbon coating on electrochemical performance of hard carbons as anode materials for lithium-ion batteries. *Journal of Power Sources* **2007,** *166*, 250–254.

[9] Zhou, G.; Pei, S.; Li, L.; Wang, D. W.; Wang, S.; Huang, K.; Yin, L. C.; Li, F.; Cheng, H. M. A

graphene-pure-sulfur sandwich structure for ultrafast, long-life lithium-sulfur batteries. *Advanced materials* **2014,** *26*, 625-631.

[10] Ji, X.; Lee, K. T.; Nazar, L. F. A highly ordered nanostructured carbon-sulfur cathode for lithium-sulfur batteries. *Nature materials* **2009,** *8*, 500–6.

[11] Xu, G. L.; Xu, Y. F.; Fang, J. C.; Peng, X. X.; Fu, F.; Huang, L.; Li, J. T.; Sun, S. G. Porous graphitic carbon loading ultra high sulfur as high-performance cathode of rechargeable lithium-sulfur batteries. *ACS applied materials & interfaces* **2013,** *5*, 10782–10793.

[12] He, G.; Evers, S.; Liang, X.; Cuisinier, M.; Garsuch, A.; Nazar, L. F. Tailoring porosity in carbon nanospheres for lithium sulfur battery cathodes. *ACS Nano* **2013,** *7*, 10920–10930.

[13] Zhang, W.; Qiao, D.; Pan, J.; Cao, Y.; Yang, H.; Ai, X. A Li^+-conductive microporous carbon–sulfur composite for Li-S batteries. *Electrochimica Acta* **2013,** *87*, 497–502.

[14] Xi, K.; Cao, S.; Peng, X.; Ducati, C.; Kumar, R. V.; Cheetham, A. K. Carbon with hierarchical pores from carbonized metal-organic frameworks for lithium sulfur batteries. *Chemical communications* **2013,** *49*, 2192–2194.

[15] Tao, X.; Chen, X.; Xia, Y.; Huang, H.; Gan, Y.; Wu, R.; Chen, F.; zhang, W. Highly mesoporous carbon foams synthesized by a facile, cost-effective and template-free pechini method for advanced lithium–sulfur batteries. *Journal of Materials Chemistry A* **2013,** *1*, 3295–3301.

[16] Brun, N.; Sakaushi, K.; Yu, L.; Giebeler, L.; Eckert, J.; Titirici, M. M. Hydrothermal carbon-based nanostructured hollow spheres as electrode materials for high-power lithium-sulfur batteries. *Physical chemistry chemical physics : PCCP* **2013,** *15*, 6080–6087.

[17] Zhang, K.; Zhao, Q.; Tao, Z.; Chen, J. Composite of sulfur impregnated in porous hollow carbon spheres as the cathode of li-s batteries with high performance. *Nano Research* **2012,** *6*, 38–46.

[18] zhou, X.; Li, L.; Dong, S.; Chen, X.; Han, P.; Xu, H.; Yao, J.; Shang, C.; Liu, Z.; Cui, G. A renewable bamboo carbon/polyaniline composite for a high-performance supercapacitor electrode material. *Journal of Solid State Electrochemistry* **2011,** *16*, 877–882.

[19] Wei, S.; Zhang, H.; Huang, Y.; Wang, W.; Xia, Y.; Yu, Z. Pig bone derived hierarchical porous carbon and its enhanced cycling performance of lithium-sulfur batteries. *Energy & Environmental Science* **2011,** *4*, 736-740.

[20] Chung, S. H.; Manthiram, A. A natural carbonized leaf as polysulfide diffusion inhibitor for high-performance lithium-sulfur battery cells. *ChemSusChem* **2014**, DOI: 10.1002/cssc.201301287.

[21] Tao, X.; Zhang, J.; Xia, Y.; Huang, H.; Du, J.; Xiao, H.; Zhang, W.; Gan, Y. Bio-inspired fabrication of carbon nanotiles for high performance cathode of Li–S batteries. *Journal of Materials Chemistry A* **2014,** *2*, 2290–2296.

[22] Moreno, N.; Caballero, A.; Hernán, L.; Morales, J. Lithium–sulfur batteries with activated carbons derived from olive stones. *Carbon* **2014,** *70*, 241-248.

[23] Tan, Z.; Sun, L.; Xiang, J.; Zeng, H.; Liu, Z.; Hu, S.; Qiu, J. Gas-phase elemental mercury removal by novel carbon-based sorbents. *Carbon* **2012,** *50*, 362–371.

[24] Kannan, N.; Sundaram, M. M. Kinetics and mechanism of removal of methylene blue by adsorption on various carbons–a comparative study. *Dyes and Pigments* **2001,** *51*, 25–40.

[25] Kim, Y. J.; Lee, B. J.; Suezaki, H.; Chino, T.; Abe, Y.; Yanagiura, T.; Park, K. C.; Endo, M. Preparation and characterization of bamboo-based activated carbons as electrode materials for electric double layer capacitors. *Carbon* **2006,** *44*, 1592–1595.

[26] Jiang, J.; Zhu, J.; Ai, W.; Fan, Z.; Shen, X.; Zou, C.; Liu, J.; Zhang, H.; Yu, T. Evolution of disposable bamboo chopsticks into uniform carbon fibers: A smart strategy to fabricate sustainable anodes for Li-ion batteries. *Energy & Environmental Science* **2014**, DOI: 10.1039/c4ee00602j.

[27] Zhang, B.; Qin, X.; Li, G. R.; Gao, X. P. Enhancement of long stability of sulfur cathode by encapsulating sulfur into micropores of carbon spheres. *Energy & Environmental Science* **2010,** *3*, 1531–1537.

[28] Wang, J.; Kaskel, S. Koh activation of carbon-based materials for energy storage. *Journal of Materials*

Chemistry **2012,** *22*, 23710–23725.

[29] Shinkarev, V. V.; Fenelonov, V. B.; Kuvshinov, G. G. Sulfur distribution on the surface of mesoporous nanofibrous carbon. *Carbon* **2003,** *41*, 295–302.

[30] Zhang, Y. Z.; Liu, S.; Li, G. C.; Li, G. R.; Gao, X. P. Sulfur/polyacrylonitrile/carbon multi-composites as cathode materials for lithium/sulfur battery in the concentrated electrolyte. *Journal of Materials Chemistry A* **2014,** *2*, 4652–4659.

[31] Zhou, G.; Yin, L. C.; Wang, D. W.; Li, L.; Pei, S.; Gentle, I. R.; Li, F.; Cheng, H. M. Fibrous hybrid of graphene and sulfur nanocrystals for high-performance lithium–sulfur batteries. *ACS Nano* **2013,** *7*, 5367–5375.

[32] Li, D.; Han, F.; Wang, S.; Cheng, F.; Sun, Q.; Li, W. C. High sulfur loading cathodes fabricated using peapodlike, large pore volume mesoporous carbon for lithium-sulfur battery. *ACS applied materials & interfaces* **2013,** *5*, 2208–2213.

[33] Zhen Li; Yan Jiang; Lixia Yuan; Ziqi Yi; Chao Wu; Yang Liu; Peter Strasser; Huang, Y. A highly ordered meso@microporous carbon-supported sulfur@smaller sulfur core-shell structured cathode for Li-S batteries. *ACS Nano***2014**, DOI: 10.1021/nn503220h.

[34] Huang, J. Q.; Liu, X. F.; Zhang, Q.; Chen, C. M.; Zhao, M. Q.; Zhang, S. M.; Zhu, W. c.; Qian, W. Z.; Wei, F. Entrapment of sulfur in hierarchical porous graphene for lithium–sulfur batteries with high rate performance from −40 to 60°c. *Nano Energy* **2013,** *2*, 314–321.

[35] Ding, B.; Yuan, C.; Shen, L.; Xu, G.; Nie, P.; Zhang, X. Encapsulating sulfur into hierarchically ordered porous carbon as a high-performance cathode for lithium-sulfur batteries. *Chemistry - A European Journal* **2013,** *19*, 1013–1019.

[36] Zhang, S. S. Sulfurized carbon: A class of cathode materials for high performance lithium/sulfur batteries. *Frontiers in Energy Research* **2013,** *1*, 1–9.

[37] Wang, Y. X.; Huang, L.; Sun, L. C.; Xie, S. Y.; Xu, G. L.; Chen, S. R.; Xu, Y. F.; Li, J. T.; Chou, S. L.; Dou, S. X. et al. Facile synthesis of a interleaved expanded graphite-embedded sulfur nanocomposite as cathode of Li-S batteries with excellent lithium storage performance. *Journal of Materials Chemistry* **2012,** *22*, 4744–4750.

[38] W. Seh, Z.; Li, W.; Cha, J. J.; Zheng, G.; Yang, Y.; McDowell, M. T.; Hsu, P. C.; Cui, Y. Sulfur-TiO_2 yolk-shell nanoarchitecture with internal void space for long-cycle lithium-sulfur batteries. *Nature communications* **2013,** *4*, 1331–1336.

[39] Wang, W. G.; Wang, X.; Tian, L. Y.; Wang, Y. L.; Ye, S. H. In situ sulfur deposition route to obtain sulfur–carbon composite cathodes for lithium–sulfur batteries. *Journal of Materials Chemistry A* **2014,** *2*, 4316–4323.

[40] Ahn, W.; Kim, K.-B.; Jung, K.-N.; Shin, K.-H.; Jin, C.-S. Synthesis and electrochemical properties of a sulfur-multi walled carbon nanotubes composite as a cathode material for lithium sulfur batteries. *Journal of Power Sources* **2012,** *202*, 394–399.

[41] Choi, H. S.; Oh, J. Y.; Park, C. R. One step synthesis of sulfur–carbon nanosheet hybrids via a solid solvothermal reaction for lithium sulfur batteries. *RSC Advances* **2014,** *4*, 3684–3690.

Electronic Supplementary Material

Microporous bamboo biochar for lithium−sulfur battery

Xingxing Gu[1], Yazhou Wang[1], Chao Lai[1], Jingxia Qiu[1], Sheng Li[1], Yanglong Hou[2](✉), Wayde Martens[3], Nasir Mahmood[2], and Shanqing Zhang[1](✉)

[1] Centre for Clean Environment and Energy, Environmental Futures Research Institute, Griffith School of Environment, Gold Coast Campus, Griffith University, QLD 4222, Australia.
[2] Department of Materials Science and Engineering, College of Engineering, Peking University, Beijing 100871, China
[3] Science and Engineering Faculty, Queensland University of Technology QLD 4001, Australia.

Supporting information to DOI 10.1007/s12274-****-****-*

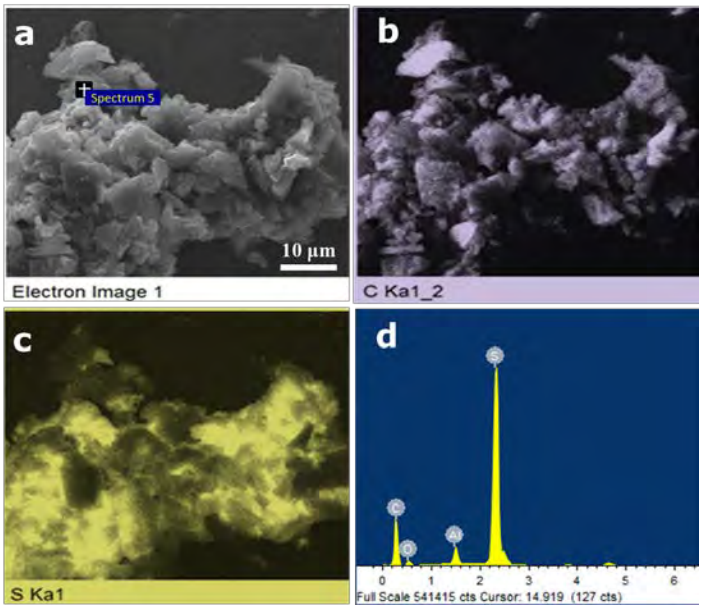

Fig. S1 SEM image of the T_BC-S-50% (a) and the EDS elemental mappings spectra of C (b), S (c) and the EDS spectrum (d) of the T_BC-S-50% sample.

Address correspondence to email1: s.zhang@griffith.edu.au; email2: hou@pku.edu.cn